ORIGINAL PAPER

Inhibition by tween-85 of the corrosion of cold rolled steel in 1.0 M hydrochloric acid solution

Xiang-Hong Li · Shu-Duan Deng · Hui Fu · Guan-Nan Mu

Abstract The inhibition effect of tween-85 on the corrosion of cold rolled steel (CRS) in 1.0 M hydrochloric acid (HCl) was studied by weight loss and potentiodynamic polarization methods. The results show that tween-85 is a good inhibitor in 1.0 M HCl and its maximum inhibition efficiency (IE) is 92% at very low concentration. Its adsorption obeys the Langmuir adsorption isotherm equation. The thermodynamic parameters of adsorption enthalpy (ΔH^0), adsorption free energy (ΔG^0) and adsorption entropy (ΔS^0) were calculated and discussed. Polarization curves show that tween-85 acts as a mixed-type inhibitor in hydrochloric acid. IE values obtained from weight loss and polarization are consistent. The adsorbed film on a CRS surface containing an optimum dose of tween-85 was investigated by Fourier transform infrared spectroscopy (FTIR), X-ray photoelectron spectroscopy (XPS) and atomic force microscope (AFM). An inhibitive mechanism is proposed from the viewpoint of adsorption theory.

X.-H. Li (✉) · H. Fu
Department of Fundamental Courses, Southwest Forestry University, Kunming 650224, People's Republic of China
e-mail: xianghong-li@163.com

S.-D. Deng
Department of Wood Science and Technology, Southwest Forestry University, Kunming 650224, People's Republic of China

G.-N. Mu
Department of Chemistry, Yunnan University, Kunming 650091, People's Republic of China

1 Introduction

The use of inhibitors is one of the most practical methods for protection against corrosion, especially in acidic media [1]. As acidic media, HCl and H_2SO_4 are widely used in the treatment of steel and ferrous alloys [2]. Inhibitors are used to prevent metal dissolution as well as acid consumption [3]. Most well known acid inhibitors are organic compounds containing nitrogen, sulfur, and oxygen atoms. Among them, the surfactant inhibitor has many advantages such as high inhibition efficiency, low cost, low toxicity and easy production [4]. Surfactants exert their inhibition action by adsorption on the metal surface such that the polar or ionic group (hydrophilic part) attaches to the metal surface while its tail (hydrophobic part) extends to the solution. The adsorption of the surfactant on the metal surface can markedly change the corrosion-resisting property of the metal [5, 6], and so the study of the relationship between adsorption and corrosion inhibition is of great importance.

Ionic surfactants have been used for the corrosion inhibition of steel [7–20], copper [21–26], aluminum [27–30] and other metals [31, 32] in different media. Recently, some nonionic surfactants have also been widely used as corrosion inhibitors for steel in acidic media [33–38]. However, data regarding the use of nonionic surfactants like the tween series are not so plentiful. The present work is an extension of earlier work on the influence of nonionic surfactant tween-85 on the inhibition of corrosion of cold rolled steel in 1.0 M HCl solution. We have reported that these non-ionic surfactants of tween series like tween-20 and tween-40 are good inhibitors in 1.0 M HCl and 1.0 M H_2SO_4 solutions [39–41]. The thermodynamic parameters of tweens reveal that the inhibition of corrosion is due to the formation of an adsorbed

film on the steel surface and their adsorption is found to follow the Langmuir adsorption isotherm. The aim of the present work is to further investigate the corrosion inhibition of another nonionic surfactant in the tween series, namely tween-85 in 1.0 M HCl. The inhibition effect of tween-85 on the corrosion of cold rolled steel was studied by weight loss and polarization methods, and the steel surface was observed by Fourier transform infrared spectroscopy (FTIR), X-ray photoelectron spectroscopy (XPS) and atomic force microscope (AFM). It is expected to further investigate the inhibitive mechanism of nonionic surfactants of tween series for steel in acidic media.

2 Experimental method

2.1 Materials

Tests were performed on a cold rolled steel (CRS) of the following composition (wt %): 0.07% C, 0.3% Mn, 0.022% P, 0.010% S, 0.01% Si, 0.030% Al, and bal. Fe.

2.2 Inhibitor

Tween-85 (Polyoxyethylene sorbitan trioleate) was obtained from Shanghai Chemical Reagent Company of China. Figure 1 shows the molecular structure of tween-85. Clearly, tween-85 is an O-heterocyclic compound with high molecular weight owing to the number of units of CH_2CH_2O.

2.3 Solutions

The aggressive solutions of 1.0 M HCl were prepared by dilution of analytical grade 37% HCl with distilled water. The concentration range of tween-85 used was 5–100 mg L^{-1}.
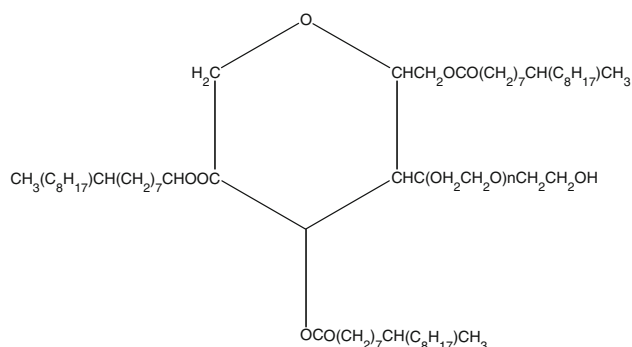

Fig. 1 The molecular structure of tween-85

2.4 Weight loss measurements

The cold rolled steel (CRS) sheets of 2.5 cm × 2.0 cm × 0.06 cm were abraded with a series of emery papers (grade 320–500–800) and then washed with distilled water and acetone. After weighing accurately, the specimens were immersed in a 250 mL beaker containing 250 mL 1.0 M HCl solution with and without addition of different concentrations of tween-85. All the aggressive acid solutions were open to air. After 6 h the specimens were taken out, washed, dried, and weighed accurately. In order to get good reproducibility experiments were carried out in triplicate. The average weight loss of three parallel CRS sheets was obtained. The tests were repeated at different temperatures. The value of corrosion rate (v) was calculated from the following equation [42]:

$$v = \frac{W}{St} \quad (1)$$

where W is the average weight loss of three parallel CRS sheets, S the total area of one CRS specimen and t is immersion time. With the calculated corrosion rate, the inhibition efficiency (IE) of tween-85 was calculated as follows [42]:

$$IE\% = \frac{v_0 - v}{v_0} \times 100 \quad (2)$$

where v_0 and v are the values of the corrosion rate without and with addition of the inhibitor, respectively.

2.5 Polarization measurements

Polarization experiments were carried out in a conventional three-electrode cell with a platinum counter electrode (CE) and a saturated calomel electrode (SCE) coupled to a fine Luggin capillary as the reference electrode. The working electrode (WE) was in the form of a square cut from CRS embedded in PVC holder using epoxy resin so that the flat surface was the only surface in the electrode. The working surface area was 1.0 cm × 1.0 cm.

Before measurement the electrode was immersed in test solution at the natural potential for 2 h until a steady state was reached. All polarization curves were recorded by a PARSTAT 2263 potentiostat (Perkin Elmer™ Company, USA) at 20 °C. The potential was increased at 30 mV min^{-1} and started from a potential of −250 mV to +250 mV vs. corrosion potential (E_{corr}). IE% was defined as:

$$IE\% = \frac{I_{corr} - I_{corr(inh)}}{I_{corr}} \times 100 \quad (3)$$

where I_{corr} and $I_{corr(inh)}$ represent the corrosion current density values without and with inhibitor, respectively.

2.6 Fourier transform infrared spectroscopy (FTIR)

FTIR spectra were recorded in an AVATAR-FTIR-360 spectrophotometer (Thermo Nicolet Company, USA). Because tween-85 is liquid, its spectrum was recorded by the OMNI Sampler accessory. In order not to damage the adsorbed protective film of the CRS surfaces after immersion in inhibited HCl solution, the FTIR reflectance accessory was applied to measure the CRS surfaces [42].

2.7 X-ray photoelectron spectroscopy (XPS)

Samples of dimension 1.0 cm × 1.0 cm × 0.06 cm were abraded with emery paper (grade 320–500–800) and washed with the same method as in section 2.4. The steel was exposed to 250 mL of 1.0 M HCl with 100 mg L^{-1} tween-85 at 20 °C for 6 h. The specimen was rinsed with distilled water and then dried in vacuum overnight.

X-ray photoelectron spectra of components, C 1s, O 1s and Fe 2p for the CRS surfaces were recorded on an X-ray photoelectron spectrometer (XPS, PHI-5500 ESCA, USA) with 200 W Mg Ka (1,253.6 eV) radiation as the source. The resolution was 0.8 eV. The base pressure in the experimental chamber was in the low 1.3×10^{-7} Pa region.

The binding energy (BE) internal calibration was referenced to the C 1s energy at 284.6 eV. Spectral decomposition assumed mixed Gaussian-Lorenzian curves and was performed by using background subtraction and a least squares fitting program.

2.8 Atomic force microscope (AFM)

The CRS specimens of size 1.0 cm × 1.0 cm × 0.06 cm were prepared as described above (Section 2.4). After immersion in 1.0 M HCl without and with addition of 100 mg L^{-1} tween-85 at 20 °C for 6 h, the specimens were cleaned with distilled water, dried with a cold air blaster and then used for Japan instrument model SPA-400 SPM Unit atomic force microscope (AFM) examinations.

3 Experimental results and discussion

3.1 Effect of tween-85 on the corrosion rate

The corrosion rate curves of cold rolled steel (CRS) with the addition of tween-85 in 1.0 M HCl at various temperatures are shown in Fig. 2. The corrosion rates (g m^{-2} h^{-1}) decrease as the concentration of inhibitor increases due to the fact that the adsorption coverage increases, which shields the CRS surface efficiently from the medium [27, 30]. Also, the curves in Fig. 2 show that the corrosion
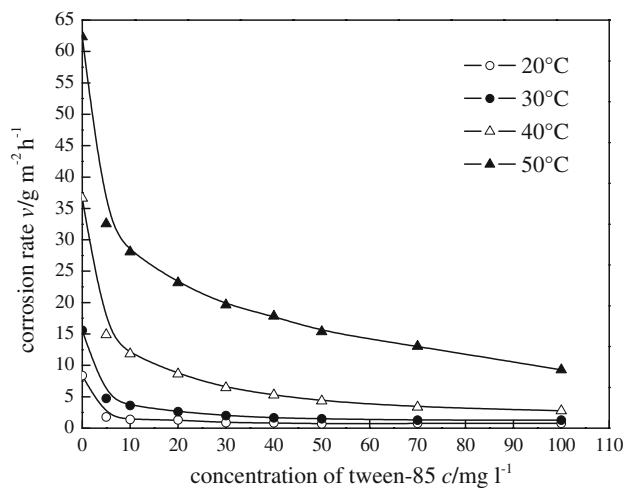

Fig. 2 Relationship between corrosion rate (v) and concentration of tween-85 (c) in 1.0 M HCl

rate increases with temperature both in uninhibited and inhibited solutions. It should be noted that the corrosion rate increases more rapidly with temperature in the absence of inhibitor. These results confirm that tween-85 acts as a good inhibitor in the range of temperature studied.

3.2 Effect of inhibitor concentration and temperature on inhibition efficiency

The values of inhibition efficiencies obtained by weight loss for different inhibitor concentrations in 1.0 M HCl are given in Fig. 3. IE increases in the inhibitor concentration range from 5 to 100 mg L^{-1}, and the maximum IE is about 92%. The inhibition was estimated to be about 79% at 20 °C even at very low concentration (5 mg L^{-1}) and at 40 mg L^{-1} its protection was higher than 90% (20–30 °C).
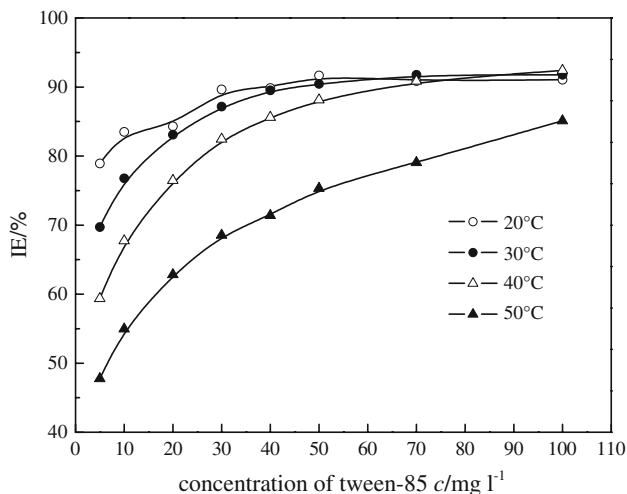

Fig. 3 Relationship between inhibition efficiency (IE) and concentration of tween-85 (c) in 1.0 M HCl

These better performances can be explained as follows. The main hydrophilic part $CHO(CH_2CH_2O)_nCH_2CH_2OH$ of tween-85 attaches to the CRS surface while the main hydrophobic part $(CH_2)_7CH(C_8H_{17})CH_3$ extends to the solution bulk. Furthermore, tween-85 adsorbs at the steel/solution interface via hydrogen bonding between the –OH groups and water molecules adsorbed on the surface. When tween-85 is adsorbed on metal surface, a coordinate bond may be formed by partial transference of electrons from the polar atom (O atom) of tween-85 to the metal surface. Also, tween-85 may be easily protonated in HCl solution, before chloride ions have a smaller degree of hydration, being specifically adsorbed. They create an excess negative charge towards the solution and favor more adsorption of the cations [43], the protonated tween-85 may adsorb through electrostatic interactions between the positively charged molecules and the negatively charged metal surface. Namely, there may be a synergism between Cl⁻ and tween-85 [41], which improves the inhibitive capability of the inhibitor.

Figure 3 also shows that the IE decreases with the temperature, which indicates that higher temperatures cause desorption of tween-85.

Using our recent work [41], in the same conditions, a comparison of the inhibition properties of tween-20 and tween-85 can be made. At 20 °C and 30 °C, IE (tween-20) >IE (twen-85) at low concentration (5–30 mg L^{-1}), while IEs of tween-20 and twen-85 are almost the same at 30–100 mg L^{-1}; But at 40 °C and 50 °C it seems that tween-85 is a better inhibitor. The difference in their inhibitive action can be explained on the basis of their molecular structure. Tween compounds are basically polyethylene glycol sorbitan combined with different fatty acids. Tween-20 (polyethylene glycol sorbitan monalaurate) and tween-85 (polyethylene glycol sorbitan trioleate) have the same hydrophilic group $CHO(CH_2CH_2O)_nCH_2CH_2OH$, but different hydrophobic groups. Consequently, the IE behavior can be attributed to the difference in the role of the hydrophobic part. Tween-20 has one hydrophobic group of $(CH_2)_{10}CH_3$, while tween-85 has three hydrophobic groups, i.e. $(CH_2)_7CH(C_8H_{17})CH_3$. The solubility in water follows the order: tween-85< tween-20. At low temperature (20 °C and 30 °C), owing to the prominent steric hindrance effect of the hydrophobic group for tween-85, compared with tween-20, adsorption is low, and it is difficult to reach saturation of the steel surface at low concentration, but when the concentration is higher than 30 mg L^{-1} the corrosion inhibition reaches a steady state for tweens. On the other hand, when the temperature increased to 40 °C and 50 °C, the solubility in water of tween-85 increased; the large hydrophobic group forms a good barrier between the metal surface and the corrosive medium. So tween-85 has better inhibition properties than tween-20.

3.3 Adsorption isotherm for tween-85

Basic information on the interaction between the inhibitor and the CRS surface can be provided by the adsorption isotherm. Attempts were made to fit experimental data to various isotherms including Frumkin, Langmuir, Temkin, Freundlich, Bockris-Swinkels and Flory-Huggins isotherms. The results were best fitted by the Langmuir adsorption isotherm equation [39–41]:

$$\frac{c}{\theta} = \frac{1}{K} + c \tag{4}$$

where c is the concentration of inhibitor, K the adsorptive equilibrium constant, and θ is the surface coverage which can be calculated by the Sekine and Hirakawa method [44]:

$$\theta = \frac{v_0 - v}{v_0 - v_m} \tag{5}$$

where v_m is the smallest corrosion rate.

From the values of surface coverage, the linear regressions between c/θ and c were calculated, and the parameters are listed in Table 1. Figure 4 shows the relationship between c/θ and c at 30 °C. These results show that all the linear correlation coefficients (r) are almost equal to 1 and all the slopes are very close to 1, which indicates that the adsorption of tween-85 obeys the Langmuir adsorption isotherm.

Table 1 Parameters of the linear regression between c/θ and c

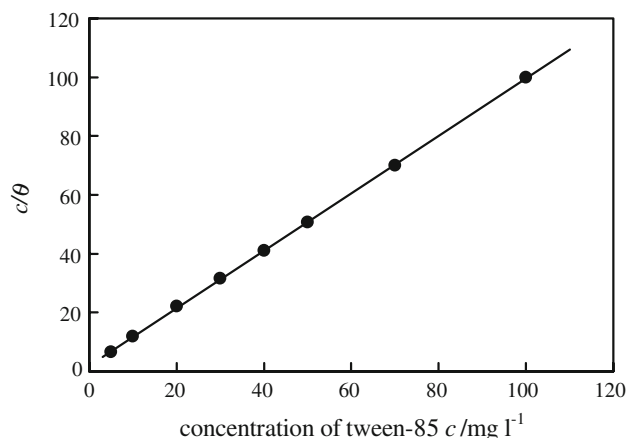| Temperature/°C	Linear correlation coefficient (r)	Slope	K/L mg^{-1}
20	0.9999	0.9937	0.9608
30	1.0000	0.9765	0.4833
40	0.9998	0.9614	0.2384
50	0.9977	0.9561	0.1394

Fig. 4 The relationship between c/θ and c at 30 °C in 1.0 M HCl

From Table 1 we can see that the adsorptive equilibrium constant (K) decreases with increase in temperature, which indicates that it is easily and strongly adsorbed onto the steel surface at relatively lower temperature. But when the temperature is relatively higher, the adsorbed inhibitor tends to desorb. In addition, large values of K mean better inhibition efficiency of the given inhibitor. This is in good agreement with the values of IE obtained from Fig. 3.

3.4 Thermodynamic parameters

Thermodynamic parameters play an important role in understanding the inhibitive mechanism. The adsorption enthalpy (ΔH) was calculated according to the Van't Hoff equation [39–41]:

$$\ln K = \frac{-\Delta H}{RT} + \text{constant} \tag{6}$$

where R is the gas constant (8.314 J K^{-1} mol^{-1}), T the absolute temperature (K).

It should be noted that $-\Delta H/R$ is the slope of the straight line $\ln K$–$1/T$ according to Eq. (6), so the value of adsorption enthalpy does not change with the unit of adsorptive equilibrium constant K. Figure 5 shows the straight line $\ln K$–$1/T$, and the linear correlation coefficient (r) is 0.9993. Because the experiment took place at standard pressure (101.3 kPa) and the solution concentration was so low that it was close to standard condition, ΔH
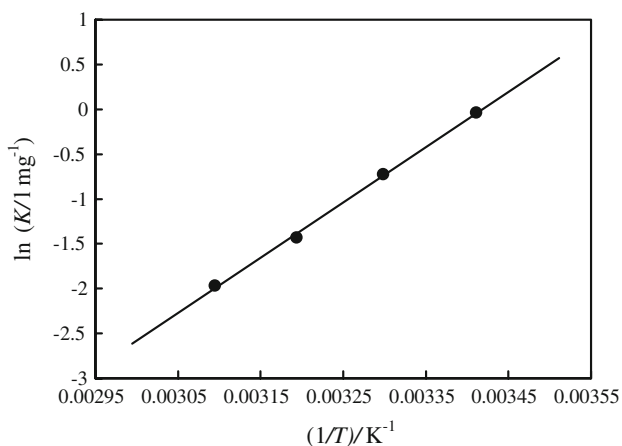

Fig. 5 The relationship between ln K and $1/T$ in 1.0 M HCl

can be approximately regarded as the standard adsorption enthalpy (ΔH^0) under the experimental conditions [27, 39–41].

The adsorptive equilibrium constant, K is related to the standard adsorption free energy (ΔG^0) obtained according to [45–47]:

$$K = \frac{1}{55.5} \exp\left(\frac{-\Delta G^0}{RT}\right) \tag{7}$$

where the value 55.5 is the concentration of water in solution expressed in M (mol L^{-1} or mol dm^{-3}) [45–47]. The unit of ΔG^0 is J mol^{-1} (or kJ mol^{-1}). Obviously, the adsorptive equilibrium constant K unit is L mol^{-1} in Eq. (7) [39, 41, 45]. Thus, the adsorptive equilibrium constant K unit L mg^{-1} (Table 1) should be changed into L mol^{-1} (or M^{-1}) [39, 41, 48]. Because tween-85 is also a polymer, it is difficult to get the exact molecular weight. We assume that the molecular weight of tween-85 is M$_w$ g mol^{-1}. The changed adsorption equilibrium constant in unit L mol^{-1} is listed in Table 2.

Then the standard adsorption entropy (ΔS^0) can be obtained by the basic thermodynamic equation:

$$\Delta S^0 = \frac{\Delta H^0 - \Delta G^0}{T} \tag{8}$$

All the calculated thermodynamic parameters are listed in Table 2. The negative value of ΔH^0 shows that the adsorption of inhibitor is an exothermic process [39], which indicates that inhibition efficiency decreases with increase in temperature. This agrees with the values of IE (Fig. 3). Such behavior can also be interpreted on the basis that the increase in temperature resulted in desorption of some adsorbed inhibitor molecules from the surface. The negative values of ΔG^0 suggest that adsorption onto the steel surface is a spontaneous process. Generally, values of ΔG^0 up to -20 kJ mol^{-1} are consistent with the electrostatic interaction between the charged molecules and the charged metal (physical adsorption) while those more negative than -40 kJ mol^{-1} involve sharing or transfer of electrons from the inhibitor molecules to the metal surface to form a co-ordinate type of bond (chemisorption) [45, 49–51]. Because the molecular weight (M$_w$) of tween-85 is about $1{,}741 \sim 1{,}917$ g mol^{-1} [52], it can be seen from Table 2 that the value of ΔG^0 is about -43 kJ mol^{-1}, which indicates that the adsorption of tween-85 on CRS

Table 2 The thermodynamic parameters of adsorption of tween-85 on the steel surface

Temperature/$^{\circ}$C	K/M^{-1}	ΔG^0/kJ mol^{-1}	ΔH^0/kJ mol^{-1}	ΔS^0/J mol^{-1} K^{-1}
20	0.9608×10^3 M$_w$	-26.53–2.48 ln M$_w$	-51.22	$-84.22 + 8.46$ ln M$_w$
30	0.4833×10^3 M$_w$	-25.70–2.52 ln M$_w$	-51.22	$-84.18 + 8.31$ ln M$_w$
40	0.2384×10^3 M$_w$	-24.71–2.60 ln M$_w$	-51.22	$-84.66 + 8.30$ ln M$_w$
50	0.1394×10^3 M$_w$	-24.06–2.69 ln M$_w$	-51.22	$-84.05 + 8.32$ ln M$_w$

* M$_w$—the molecular weight of tween-85, $1741 \sim 1917$ g mol^{-1}

involves chemisorption. Thus the adsorption of tween-85 onto the steel surface can be explained on the basis of donor-acceptor interaction between the lone pairs of electrons of oxygen atoms and the vacant d orbital of iron surface atoms. As for the value of ΔS^0 in Table 2, the sign of ΔS^0 is negative, which mean that the process of adsorption is accompanied by a decrease in entropy. This may be explained as follows: before the adsorption of tween-85 onto the steel surface, the chaotic degree of steel/solution interface surface is high, but when inhibitor molecules are adsorbed onto the steel surface there is increased order and a resultant decrease in entropy.

3.5 Polarization studies

Both anodic and cathodic polarization curves for CRS in 1.0 M HCl at various concentrations of tween-85 are shown in Fig. 6. The presence of inhibitor causes a remarkable decrease in the corrosion rate i.e. shifts the anodic curves to more positive potentials and the cathodic curves to more negative potentials. This may be ascribed to adsorption of inhibitor over the corroded surface [53]. Figure 6 also shows that the strong polarization (beyond $E_{corr} \pm 120$ mV) curves deviate from Tafel lines owing to significant change in the surface state of electrodes. According to Li and Gu [54], the optimum weak polarization region is −50 to −10 mV (vs. E_{corr}) and 10 to
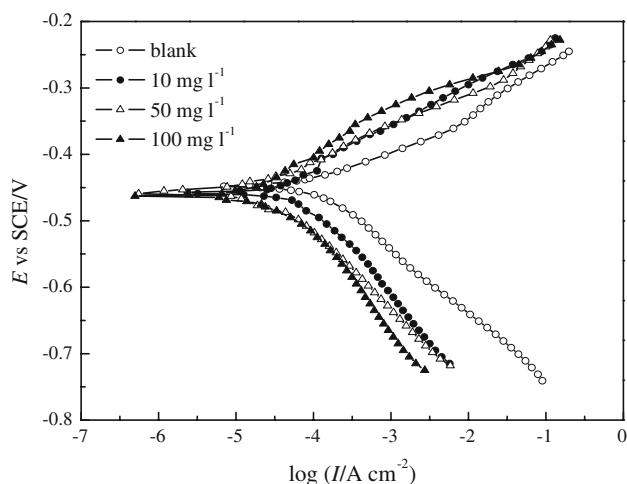
Fig. 6 Potentiodynamic polarization curves for CRS in 1.0 M HCl containing tween-85 at 20 °C

50 mV (vs. E_{corr}). However, Shi and Song [55] consider the results obtained by fitting the region of −50 to −10 mV (vs. E_{corr}) and 10 to 50 mV (vs. E_{corr}) could suffer from their sensitivity to measuring errors owing to use of only a few data points. Therefore, in the present paper, the corrosion parameters including corrosion current density (I_{corr}), corrosion potential (E_{corr}), the cathodic Tafel slope (b_c), and anodic Tafel slope (b_a) were calculated by fitting the weak Tafel polarization curves in the optimum region of $E_{corr} \pm 120$ mV. With the corrosion current densities (I_{corr}), the inhibition efficiency (IE) was calculated according to Eq. (3). All the results of corrosion parameters and IE are listed in Table 3.

Table 3 shows that I_{corr} decreases remarkably and IE increases with inhibitor concentration. The presence of tween-85 does not prominently shift the corrosion potential, which indicates that tween-85 acts as a mixed-type inhibitor in HCl and the inhibition category belongs to geometric blocking [56, 57]. Both b_a and b_c change upon addition of tween-85, which indicates that the inhibitor affects both anodic and cathodic reactions [53]. Furthermore, the inhibition efficiencies obtained from weight loss and electrochemical polarization curves are in reasonably good agreement.

3.6 Fourier transform infrared spectroscopy (FTIR)

Several researchers [9, 58–60] have confirmed that FTIR spectrometry is a powerful tool that can be used to determine the type of bonding for organic inhibitors. In this paper, FTIR spectrometry was used to identify whether there was adsorption and to provide new bonding information on the steel surface after immersion in inhibited HCl solution.

The FTIR spectrum of pure tween-85 is shown in Fig. 7a. The band at 3,474 cm^{-1} is attributed to O–H stretching and that at 1,735 cm^{-1} to C=O. The bands at 2,922 and 2,861 cm^{-1} are attributed to the aliphatic –CH$_2$ asymmetric and symmetric stretching vibrations, respectively. The absorption bands at 1,645 and 1,458 cm^{-1} are due to the framework vibration of O-heterocyclic ring. The band at 1,353 cm^{-1} is attributed to C–H bending in –CH$_3$ and –CH$_2$. Besides these, there is a strong peak band at 1,105 cm^{-1}, which may be assigned to the C–O–C asymmetric stretching vibration in the ester bond (O–C=O) [61].

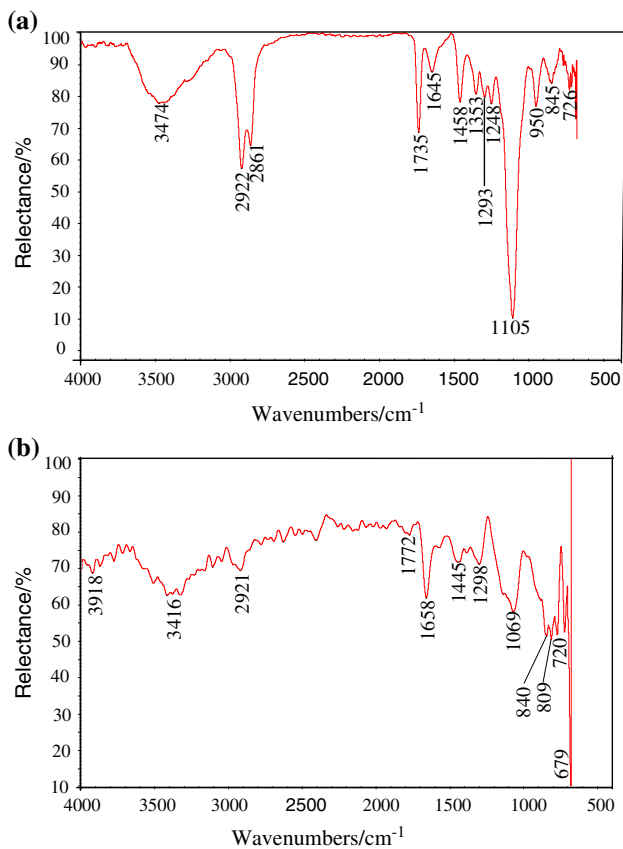| c/mg L^{-1}	E_{corr} vs SCE/mV	I_{corr}/µA cm^{-2}	b_c/mV dec^{-1}	b_a/mV dec^{-1}	IE/%
0	−447.3	132.9	103	62	–
10	−449.3	24.8	137	85	81.3
50	−456.4	17.7	115	72	86.7
100	−457.4	14.5	126	70	89.1

Table 3 Potentiodynamic polarization parameters for the corrosion of cold rolled steel in 1.0 M HCl containing different concentration of tween-85 at 20 °C

Fig. 7 FTIR spectra of (a) tween-85 (b) the CRS surface after immersion in 1.0 M HCl + 100 mg L^{-1} tween-85

The band at 950 cm^{-1} is attributed to symmetrical extension vibration of C–O–C in (CH$_2$CH$_2$O)$_n$ and that at 726 cm^{-1} is due to plane vibration of (–CH$_2$–)$_n$ ($n > 4$).

The FTIR reflectance spectrum of CRS after immersion in 1.0 M HCl containing 100 mg L^{-1} tween-85 is shown in Fig. 7b. The weak band at 3,918 cm^{-1} is attributed to Fe–O bending, which indicate that a coordinate bond is formed by partial transference of electrons from the polar atom (O atom) of tween-85 to the metal surface. The band at 3,416 cm^{-1} is attributed to O–H stretching and 1,658 cm^{-1} is for O–H bending. The band at 2,921 cm^{-1} is attributed to O=C–O bending. The band at 1,772 cm^{-1} is attributed to C=O and that at 1,445 cm^{-1} is due to –CH$_2$ bending. In addition, it should be noted that the band at 1,069 cm^{-1} is the asymmetric stretching vibration in C–O–C. Comparing Fig. 7a and b, it can be suggested that tween-85 is absorbed on the steel surface.

3.7 X-ray photoelectron spectroscopy (XPS)

In order to further confirm the assumption that the inhibitor of tween-85 adsorbs on the steel surface in 1.0 M HCl, XPS was also studied. The presence of tween-85 on the steel surface was monitored using the characteristic C 1s, O 1s and Fe 2p signals. The XPS spectra were obtained from the steel surface treated by 100 mg L^{-1} tween-85 after 6 h of immersion in 1.0 M HCl at 20 °C. It can be seen from Fig. 8 that it contains Fe, O, C and adventitious contaminates such as Ca. Figure 9 is the high resolution spectra of the C 1s peak. Four peaks are evident independently of the microstructure: 284.8 eV, 286.4 eV, 288.2 eV and 289.4 eV. The peak of BE at 284.8 eV is related to the presence of cementite (Fe$_3$C) [62]. The BE at 286.4 eV corresponds to residual or adventitious carbon [63, 64]. The peak at 288.2 eV is due to C=O and the peak at the highest binding energy of 289.4 eV is due to O–C=O or the complex of Fe •••C=O, which may indicate that the organic inhibitor (tween-85) is adsorbed.

Figure 10 presents the O 1s high resolution XPS spectra. Three distinct peaks are observed: the one at the lowest binding energy at 529.5 eV represents the oxide bond (MO), the 531.1 eV peak due to metal hydroxide (MOH) [65]. Ramji et al. [66] suggested the peak at the binding energy of 532.5 ± 0.2 eV is due to another tween series of tween-80. Accordingly, the highest binding energy of

Fig. 8 Survey spectra of XPS analysis for CRS surface exposed to a (1.0 M HCl + 100 mg L^{-1} tween-85) solution for 6 h at 20 °C
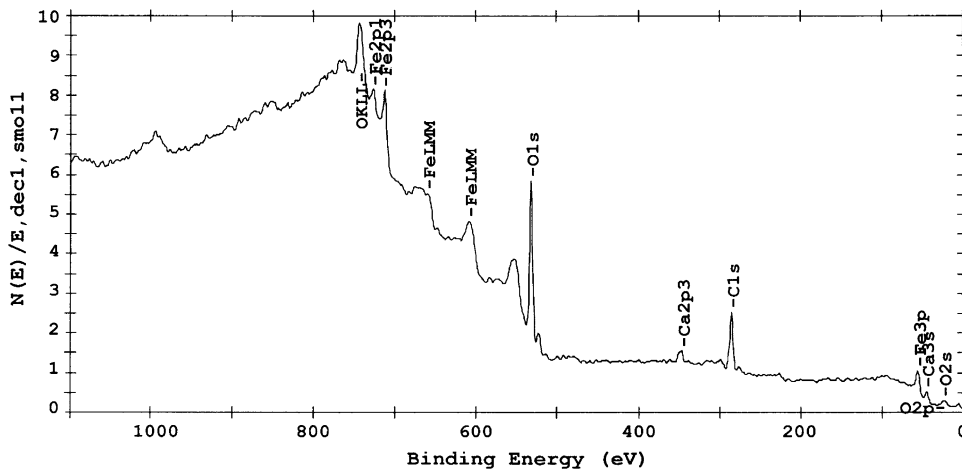
Fig. 9 High resolution C 1s spectra of XPS analysis for CRS surface exposed to a (1.0 M HCl + 100 mg L^{-1} tween-85) solution for 6 h at 20 °C
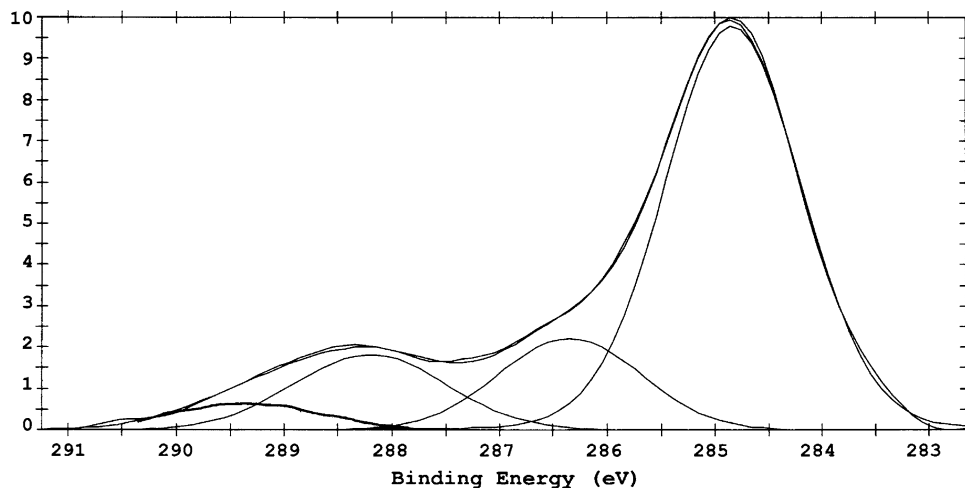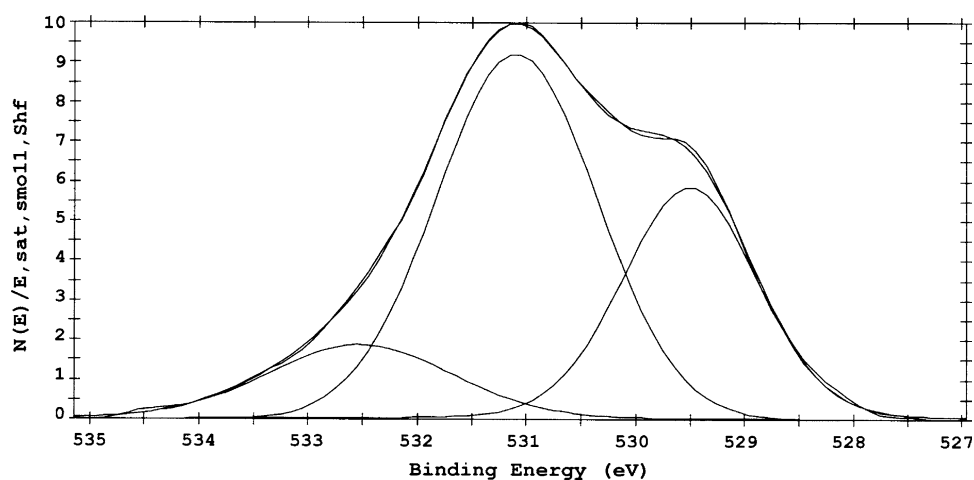

Fig. 10 High resolution O 1s spectra of XPS analysis for CRS surface exposed to a (1.0 M HCl + 100 mg L^{-1} tween-85) solution for 6 h at 20 °C

532.8 eV may due to tween-85. The existence of an oxygen peak corresponding to tween-85 in the O 1s spectra of steel treated with its optimum concentration confirmed the adsorption of tween-85 molecules on the steel surface. There are two kinds of oxygen atom in the tween-85 molecule.

The XPS spectra for the Fe 2p region are shown in Fig. 11. The two main signals located at around 724.5 and 711.4 eV can be ascribed to the photoemission peaks from Fe 2p$_{1/2}$ and Fe 2p$_{3/2}$, which means that a certain degree of oxidation of Fe occurs. According to literature [42], the CRS before immersion shows a peak for Fe 2p at BE

Fig. 11 Fe 2p spectra for CRS surface exposed to a (1.0 M HCl + 100 mg L^{-1} tween-85) solution for 6 h at 20 °C
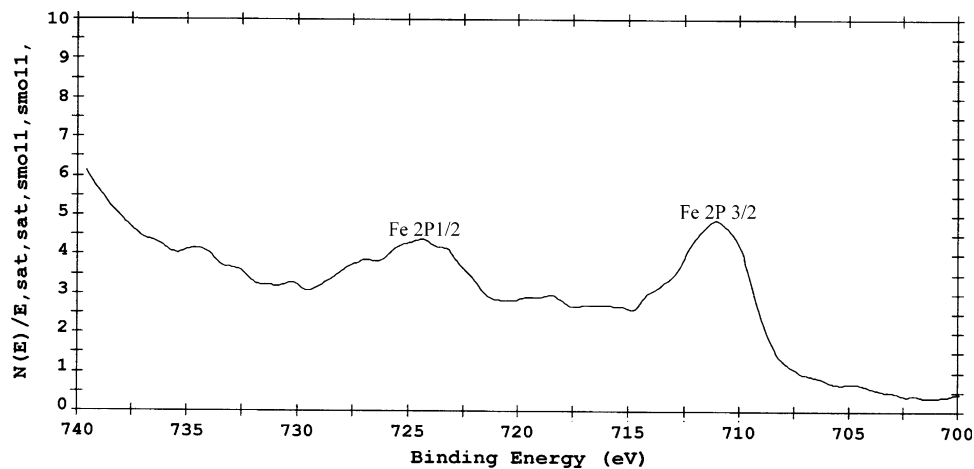
707.4 eV characteristic of Fe^0. In comparison with the CRS before immersion, immersion in HCl solution containing tween-85 induces an increase in the Fe 2p signal, also confirming adsorption and film formation on the steel surface [67].

3.8 Atomic force microscope (AFM) surface examination

The atomic force microscope (AFM) provides a powerful means of characterizing the microstructure [68–71]. Figure 12 illustrates the corresponding two-dimensional AFM phase images. Figure 13 shows the CRS surface topography in 1.0 M HCl. Both phase image and topography image give similar surface features. The main differences between phase image and topography image are two points: (i) Compared with the topography image, the phase image affords greater resolution for sample features, by which the particle images can be distinguished on the micro-nanometer scale. Accordingly, the main aim of the phase image is to distinguish the particle image. (ii) In comparison with the phase image, the main aim of the

topography image is to distinguish the surface roughness and visualize the arrangement of particles.

As can be seen from Fig. 12(a), the CRS surface after immersion in uninhibited 1.0 M HCl for 6 h shows an aggressive attack of the corroding medium on the steel surface, and its coverage with corrosion products. However, corrosion appears to be relatively uniform with no evident black holes or crevices. The image is quite different from the pitting corrosion image [70] or corrosion in $HClO_4$-CH_3COOH solution [72]. On the other hand, in the presence of tween-85 inhibitor, Fig. 12(b) shows that the steel surface appears smoother, homogeneous and uniform, which indicates that tween-85 provides significant resistance to corrosion. In addition, some compact spherical or bead-like particles appear on the surface in the presence of 100 mg L^{-1} tween-85, which do not exist in Fig. 12(a). Similar results are also reported in our recent studies for tween-20 and tween-40 inhibitor in acid [39–41]. Thus it may be concluded that these particles are the adsorption film which efficiently inhibits the corrosion of steel [39–41].

Figure 14 illustrates the height profiles made along the line marked in the corresponding Fig. 13. It can be seen from

Fig. 12 AFM two-dimensional phase images of the cold rolled steel (CRS) surface in 1.0 M HCl: a in the absence of tween-85; b in the presence of 100 mg L^{-1} tween-85
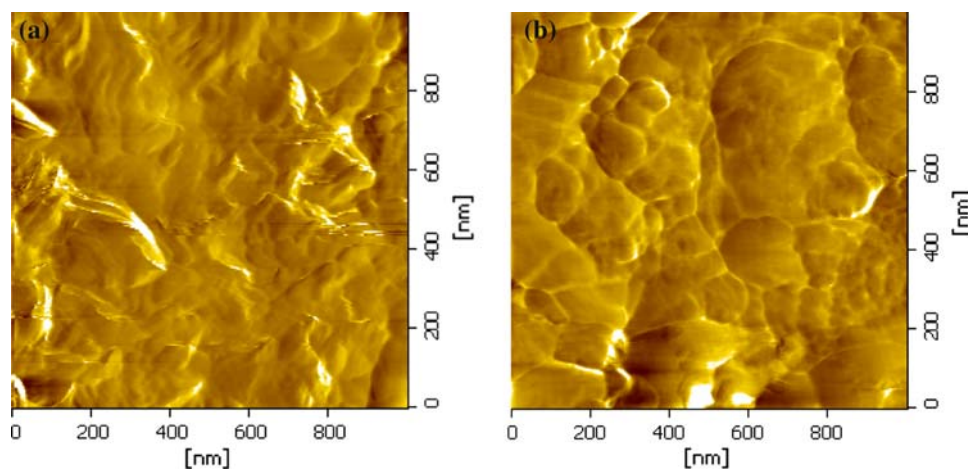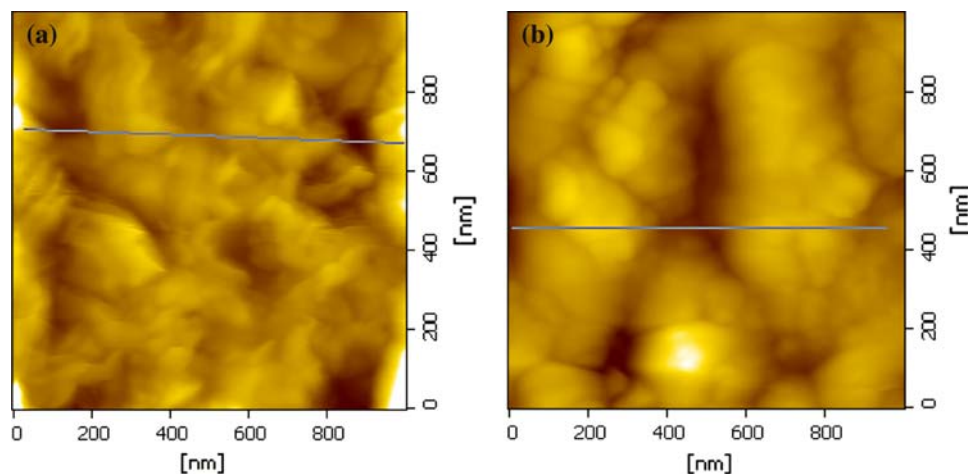

Fig. 13 AFM topography images of the cold rolled steel (CRS) surface in 1.0 M HCl: a in the absence of tween-85; b in the presence of 100 mg L^{-1} tween-85
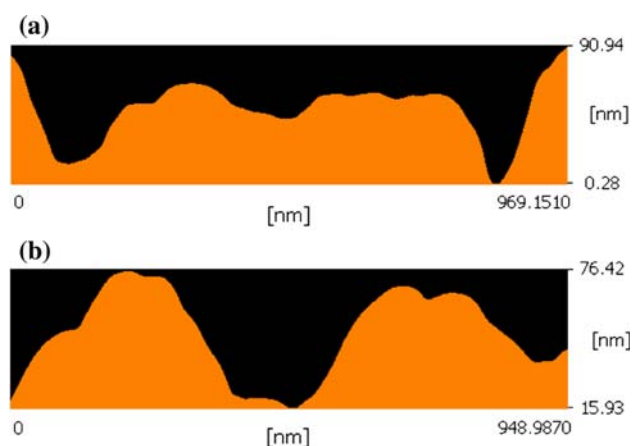
Fig. 14 Height profiles of the CRS surface in 1.0 M HCl: **a** in the absence of tween-85; **b** in the presence of 100 mg L^{-1} tween-85

Fig. 13(a) that the micrograph of the CRS surface after immersion in uninhibited 1.0 M HCl shows corrosion products appearing at edges and corners. From Fig. 13(b) we can see that some spherical and bead-like particles are distributed on the surface, which indicates the formation of a microscopically thin film [39–41]. Figure 13(b) also shows that the particles provide fully ordered covering on the steel surface after adding tween-85 in 1.0 M HCl. Figure 14(a) shows that the surface roughness of the CRS in uninhibited 1.0 M HCl is about 90.66 nm, while in the presence of tween-85, it decreases to 60.49 nm (Fig. 14(b)). Moreover, the roughness is consistent with the results shown in Figs. 12–13. These results reveal that there is a good protective film adsorbed on the specimen surface exposed to 1.0 M HCl solution containing tween-85.

4 Conclusion

1. Tween-85 acts as a good inhibitor for the corrosion of CRS in 1.0 M HCl and its maximum IE is about 92%. The IE values increase with inhibitor concentration, while they decrease with temperature.
2. The adsorption of the tween-85 on the CRS surface obeys the Langmuir adsorption isotherm. The adsorption process is spontaneous and exothermic and is accompanied by a decrease in entropy.
3. Tween-85 acts as a mixed-type inhibitor in 1.0 M HCl. The results obtained from weight loss and polarization curves are in reasonably good agreement.
4. FTIR, XPS and AFM results reveal that the introduction of tween-85 into 1.0 M HCl solution results in the formation of an adsorbed protective film on the CRS surface, which causes ta decrease in the steel surface roughness and effectively protects the steel from corrosion.

References

1. Trabanelli G (1991) Corrosion 47:410
2. Lebrini M, Lagrenée M, Traisnel M, Gengembre L, Vezin H, Bentiss F (2007) Appl Surf Sci 253:9276
3. ElAzhar M, Mernari B, Traisnel M, Bentiss F, Lagrenée M (2001) Corros Sci 43:2229
4. Tizpar A, Ghasemi Z (2006) Appl Surf Sci 252:8630
5. Free ML (2002) Corros Sci 44:2865
6. Atia AA, Saleh MM (2003) J Appl Electrochem 33:171
7. Hajjaji N, Ricco I, Srhiri A, Lattes A, Soufiaoui M, BenBachir A (1993) Corrosion 49:326
8. Elachouri M, Hajji MS, Salem M, Kertit S, Coudert R, Essassi EM (1995) Corros Sci 37:381
9. Luo H, Guan YC, Han KN (1998) Corrosion 54:619
10. Migahed MA, Azzam EMS, Al-Sabagh AM (2004) Mater Chem Phys 85:273
11. Osman MM, Omar AM, Al-Sabagh AM (1997) Mater Chem Phys 50:271
12. Zucchi F, Trabanelli G, Brunoro G (1992) Corros Sci 33:1135
13. Elachouri M, Hajji MS, Kertit S, Essassi EM, Salem M, Coudert R (1994) Corros Sci 37:381
14. Wei Z, Duby P, Somasundaran P (2003) J Colloid Interface Sci 259:97
15. Bastidas JM, Polo JL, Cano E, Torre CL (2000) J Mat Sci 35:2637
16. Bastidas JM, Polo JL, Cano E (2000) J Appl Electrochem 30:1173
17. Abdel Hamid Z, Soror TY, El Dahan HA, Omar AM (1998) Anti-Corros Methods Mater 45:306
18. Saleh M, Atia AA (2006) J Appl Electrochem 36:899
19. Migahed MA (2005) Mater Chem Phys 93:48
20. Al Sabagh AM, Migahed MA, Awad HS (2006) Corros Sci 48:813
21. Maayta AK, Bitar MB, Al-Abdallah MM (2001) Br Corros J 36:133
22. Villamil RFV, Corio P, Rubim JC, Silvia Agostinho ML (1999) J Electroanal Chem 472:112
23. Fuchs-Godec R, Dolecek V (2004) Colloids Surf A 244:73
24. Ma H, Chen S, Yin B, Zhao S, Liu X (2003) Corros Sci 45:867
25. Amin AA (2006) J Appl Electrochem 36:215
26. Zhan DQ, Gao LX, Zhou GD, Lee KY (2008) J Appl Electrochem 38:71
27. Zhao TP, Mu GN (1999) Corros Sci 41:1937
28. Abd El Rehim SS, Hassaan HH, Amin MA (2001) Mater Chem Phys 70:64
29. Abd El Rehim SS, Hassaan HH, Amin MA (2002) Mater Chem Phys 78:337
30. Maayta AK, Al-Rawashdeh NAF (2004) Corros Sci 46:1129
31. Guo R, Liu T, Wei X (2002) Colloids Surf A 209:37
32. Branzoi V, Golgovici F, Branzoi F (2002) Mater Chem Phys 78:122
33. Elachouri M, Hajji MS, Salem M, Kertit S, Aride J, Coudert R, Essassi E (1996) Corrosion 52:103
34. Algaber AS, El-Nemma EM, Saleh MM (2004) Mater Chem Phys 86:26
35. Osman MM, Shalaby MN (1997) Anti-Corros Methods Mater 44:318
36. Migahed MA, Abd El Raouf M, Al Sabagh AM, Abd El Bary HM (2005) Electrochim Acta 50:4683
37. Migahed MA, Abd El Raouf M, Al Sabagh AM, Abd El Bary HM (2006) J Appl Electrochem 36:395
38. Fuchs-Godec R (2007) Electrochim Acta 52:4974
39. Li XH, Mu GN (2005) Appl Surf Sci 252:1254
40. Mu GN, Li XH (2005) J Colloid Interface Sci 289:184
41. Li XH, Deng SD, Mu GN, Fu H, Yang FZ (2008) Corros Sci 50:420

42. Li XH, Deng SD, Fu H, Mu GN, Zhao N (2008) Appl Surf Sci 254:5574
43. Bentiss F, Traisnel M, Chaibi N, Mernari B, Vezin H, Lagrenée M (2002) Corros Sci 44:2271
44. Sekine I, Hirakawa Y (1986) Corrosion 42:272
45. Li WH, He Q, Zhang ST, Pei CL, Hou BR (2008) J Appl Electrochem 38:289
46. Khamis E (1990) Corrosion 46:476
47. Moretti G, Guidi F, Grion G (2004) Corros Sci 46:387
48. Li GM (2003) Anti-Corros Meth Mater 50:410
49. Kamis E, Bellucci F, Latanision RM, El-Ashry ESH (1991) Corrosion 47:677
50. Bensajjay E, Alehyen S, El Achouri M, Kertit S (2003) Anti-Corros Meth Mater 50:402
51. Bentiss F, Lebrini M, Lagrenée M (2005) Corros Sci 47:2915
52. Committee of Chinese Industrial Engineering (2003) Dictionary of Chemical Technology. Chemical Industrial Engineering Press, Beijing, p 1283 (in Chinese)
53. Mu GN, Li XH, Qu Q, Zhou J (2006) Corros Sci 48:445
54. Li CM, Gu N (1998) Mater Prot 31(6):25 (in Chinese)
55. Shi XM, Song SZ (2005) 16th International Corrosion Congress, Beijing, China, paper number 14-01
56. Cao CN (1996) Corros Sci 38:2073
57. Cao CN (2004) Corrosion Electrochemistry. Chemical Engineering Press, Beijing, p 235 (in Chinese)
58. Lalitha A, Ramesh S, Rajeswari S (2005) Electrochim Acta 51:47
59. Qu Q, Jiang SA, Bai W, Li L (2007) Electrochim Acta 52:6811
60. Manov S, Lamazouère AM, Ariès L (2000) Corros Sci 42:1235
61. Zhang XF, Cheng XN, Yin HB, Wu YY (2007) Chin J Nonferrous Metals 17:1700 (in Chinese)
62. Park E, Zhang J, Thomson S, Ostrousky O, Howe R (2001) Metall Trans B 32:839
63. López DA, Schreiner WH, de Sánchez SR, Simison SN (2004) Appl Surf Sci 236:77
64. Wagner CD, Riggs WM, Davis LE, Moulder JF, Muilenberg GE (eds) (1979) Handbook of X-ray photoelectron spectroscopy. Perkin Elmer Corporation (Physical Electronics), Eden Prairie, Minnesota
65. Baghmi IM, Lyon SB, Ding B (2004) Surf Coat Tech 185:194
66. Ramji K, Cairns DR, Rajeswari S (2008) Appl Surf Sci 254:4483
67. Bentiss F, Lagrenée M, Traisnel M (2000) Corrosion 56:733
68. Gewirth AA, Niece BK (1997) Chem Rev 97:1129
69. Oppenherm IC, Trevor D, Chidsey CED, Trevor PL, Sieradzki K (1991) Science 254:688
70. Li J, Lampner D (1999) Colloids Surf A 154:227
71. Teng HH, Dove PM, Orme CA, De Yoreo JJ (1998) Science 282:724
72. Huang CA, Lin W, Lin SC (2003) Corros Sci 45:2627